

Wavelet Imaging Cleaning Method for Atmospheric Cherenkov Telescopes

R.W. Lessard ^{a,1} L. Cayón ^b G.H. Sembroski ^a J.A. Gaidos ^a

^a*Department of Physics, Purdue University, West Lafayette, IN, 47907, USA*

^b*Instituto de Física de Cantabria, Fac. Ciencias, avda. Los Castros s/n, 39005 Santander, Spain*

Abstract

We present a new method of image cleaning for imaging atmospheric Cherenkov telescopes. The method is based on the utilization of wavelets to identify noise pixels in images of gamma-ray and hadronic induced air showers. This method selects more signal pixels with Cherenkov photons than traditional image processing techniques. In addition, the method is equally efficient at rejecting pixels with noise alone. The inclusion of more signal pixels in an image of an air shower allows for a more accurate reconstruction, especially at lower gamma-ray energies that produce low levels of light. We present the results of Monte Carlo simulations of gamma-ray and hadronic air showers which show improved angular resolution using this cleaning procedure. Data from the Whipple Observatory's 10-m telescope are utilized to show the efficacy of the method for extracting a gamma-ray signal from the background of hadronic generated images.

Key words: Gamma-ray astronomy; Atmospheric Cherenkov Technique; Wavelets

1 Introduction

The study of astrophysical sources of very high energy (VHE, $E > 100$ GeV) gamma rays was revolutionized by the development of the Imaging Atmospheric Cherenkov technique (ACT), pioneered by the Whipple Gamma-ray Collaboration in the late 1980s. The Collaboration utilizes a 10-m optical reflector and camera consisting of an array of closely packed photomultiplier tubes (PMTs) mounted in the focal plane. The camera detects Cherenkov

¹ Current address - Merak Projects, Ltd., 600, 322 11th Ave. S.W., Calgary, Alberta, Canada, T2R 0C5

radiation produced by gamma-ray and cosmic-ray air showers from which an image of the Cherenkov shower can be reconstructed. The reflector, located at the Fred Lawrence Whipple Observatory on Mt. Hopkins (elevation 2320 m) in southern Arizona, was the first instrument to detect a VHE gamma-ray signal from the Crab Nebula with high significance (1). Since then numerous modifications have been made to improve the sensitivity and performance of the system which has been used as the model for many additional observatories throughout the world.

The advancement of the ACT over the past decade has been directed towards detecting lower energy gamma-rays, thereby closing the gap between space-based instruments and ground-based observatories, and improving the sensitivity to weaker gamma-ray sources. This has been accomplished by utilizing finer pixellated cameras, faster electronics and more intelligent triggering systems, for example the GRANITE III upgrade of the Whipple Observatory's 10-m gamma-ray telescope (2; 3) and the Cherenkov at Thémis (CAT) telescope in the French Pyrenees (4). The push towards lower energy thresholds has presented new challenges for the ACT. Firstly, the lower light levels associated with low energy gamma-ray air showers resulted in significant sensitivity to Cherenkov light from single local muons (5). Secondly, the small images recorded from low energy showers cover only a few pixels making image reconstruction less precise (6). Recent efforts in ACT have been directed towards resolving these challenges. We present in this paper a novel method based on wavelets to enhance the image processing technique.

The paper is organised as follows. Section 2 provides an introduction to the imaging atmospheric Cherenkov technique and the traditional method used for image processing. The novel image processing method based on wavelets is presented in Section 3. A comparison with the traditional method is also discussed towards the end of that section. The effects of traditional cleaning versus wavelet cleaning on image reconstruction and characterization, are presented in Section 4. Conclusions are included in Section 5.

2 Imaging Atmospheric Cherenkov Technique

Primary cosmic rays and gamma rays entering the atmosphere initiate showers of secondary particles which propagate towards the ground. The trajectory of the shower continues along the path of the primary particle. If the optical reflector lies within the 300 m diameter Cherenkov light pool, it forms an image in the PMT camera. The appearance of this image depends upon a number of factors. The nature and energy of the incident particle, the arrival direction and the point of impact of the particle trajectory on the ground, all determine the initial shape and orientation of the image. This image is modified by the

point spread function of the telescope, the addition of instrumental noise in the PMTs and subsequent electronics, the presence of bright stellar images in certain PMTs, the diffuse night sky background and by spurious signals from charged cosmic rays physically passing through the tubes. Monte Carlo studies have shown that gamma-ray induced showers give rise to more compact images than background hadronic showers and are preferentially oriented towards the source position in the image plane (7). By making use of these differences, a gamma-ray signal can be extracted from the large background of hadronic showers and a gamma-ray map over the field of view (FOV) can be obtained. The method of extracting a gamma-ray signal from the hadronic background can be found in (8).

2.1 *Traditional Image Processing*

Prior to analysis of the recorded images, two calibration operations must be performed: the subtraction of the pedestal analog-digital conversion (ADC) values and the normalization of the PMT gains, a process known as flat-fielding.

The pedestal of an ADC is the finite value which it outputs for an input without signal from genuine showers. This is usually set at 20 digital counts so that small negative fluctuations on the signal line, due to night sky noise variations, will not generate negative values in the ADC. The pedestal for each PMT is determined by artificially triggering the camera, thereby capturing ADC values in the absence of genuine input signals. The PMT pedestal and pedestal variance are calculated from the mean and variance of the pulse-height spectrum generated from these injected events.

The relative PMT gains are determined by recording a thousand images using a fast Optitron Nitrogen Arc Lamp illuminating the focal plane through a diffuser. These nitrogen pulser images are used to determine the relative gains by comparing the relative mean signals seen by each PMT.

Fluctuations in the image usually arise from electronic noise and night-sky background variations. The traditional method to reject these distortions was developed for a camera consisting of 109 PMTs (each viewing a circular field of 0.259° diameter) utilized by the Whipple Observatory's 10-m gamma-ray telescope. The method selects a PMT to be part of the image if it has a signal above a certain threshold or is beside such a PMT and has a signal above a lower threshold. These two thresholds are defined as the picture and boundary thresholds, respectively. The picture and boundary thresholds are multiples of the root mean square (RMS) pedestal deviation which PMT's signal must exceed to be considered part of the picture or boundary, respectively. The

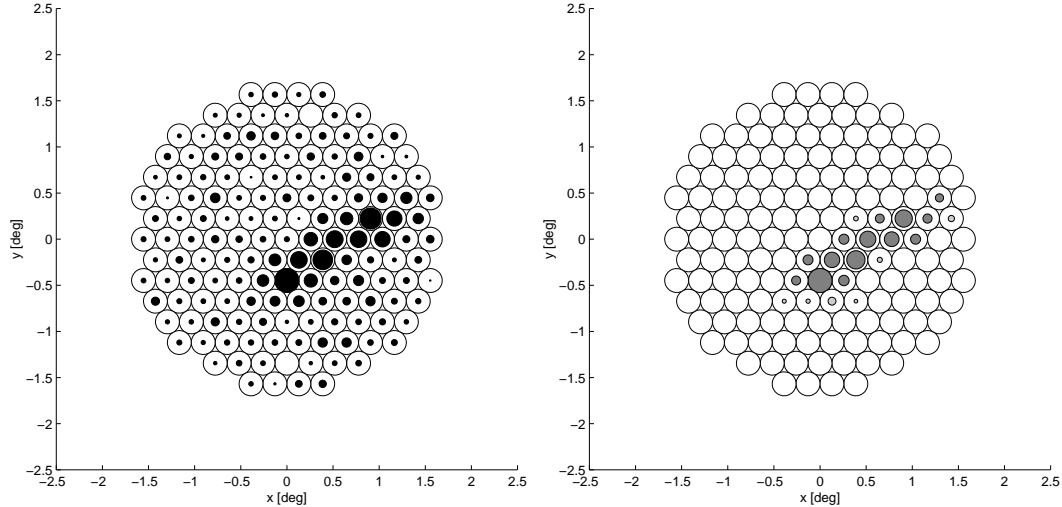


Fig. 1. (Left) Example of an image prior to the processing procedure given in the text. Diameter of each filled circle is proportional to the ADC signal for that PMT. (Right) The same image after pedestal subtraction, application of picture (dark gray filled circles) and boundary (light gray filled circles) thresholds and gain normalization.

picture and boundary PMTs together make up the image; all others are zeroed. This image cleaning procedure is depicted in Figure 1. A picture threshold of $4.25 \times \text{RMS}$ and a boundary threshold of $2.25 \times \text{RMS}$ were chosen to select the greatest number of PMTs with signal while at the same time limiting the inclusion of PMTs with noise alone.

Monte Carlo simulations of gamma-ray induced air showers are used to test the performance of these imaging procedures. The simulations track each particle produced in the air shower and trace each Cherenkov photon emitted to the image plane. Included in the simulation are the effects of the atmosphere, mirror alignment and reflectivity, and the quantum efficiency of the PMTs. Background light from the night sky and electronic noise are added to match the conditions present during the course of typical observations. These simulations, described in (9), are utilized by the Collaboration to determine the energy dependent collection area of the Whipple 10-m telescope as presented in (10).

Figure 2 shows two sample images of Monte Carlo simulated showers initiated by 150 GeV gamma-rays. The x symbols indicate PMTs with at least one photoelectron due to Cherenkov light from the shower. The pixels selected by the traditional picture and boundary threshold method are shown in gray scale with darker shades corresponding to greater ADC signal for that PMT. For the image on the top left, 25% of the PMTs with Cherenkov signal are selected by the cleaning process. The image on the top right was chosen to show an example where very few pixels are selected by the standard cleaning method. In this case just three pixels or 7% of the PMTs with signal were

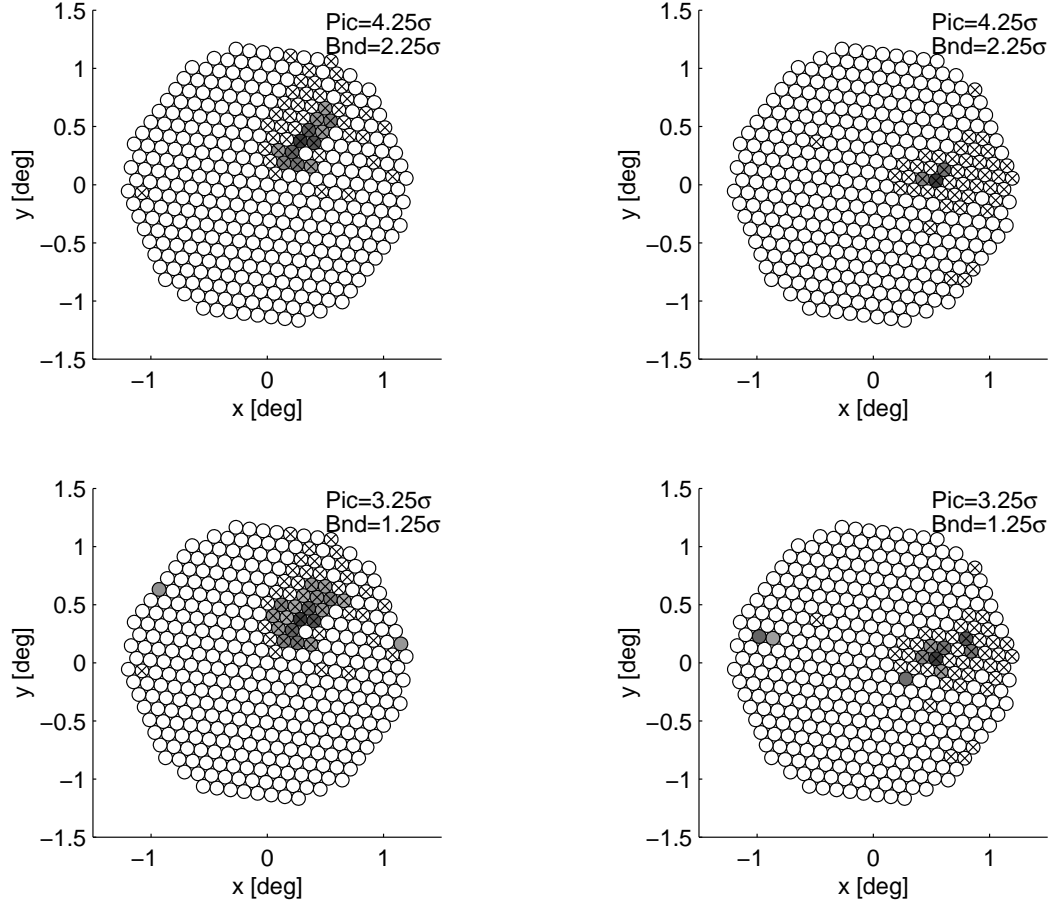


Fig. 2. (Top) Two examples of images cleaned using the traditional method of picture and boundary thresholds given in the text. Pixels selected by this technique are shaded in gray scale with darker shades corresponding to greater ADC signal for that PMT. The x symbols indicate pixels with at least one photoelectron due to Cherenkov light. (Bottom) The same images but cleaned using lower picture and boundary thresholds.

selected. By lowering the picture and boundary thresholds we can accept more signal PMTs, as shown in the bottom panels of Figure 2 which depict the same images given in the top panels but cleaned with picture and boundary thresholds of $3.25 \times \text{RMS}$ and $1.25 \times \text{RMS}$ respectively. However, the number of noise PMTs selected with the lower thresholds also increases. The goal of the image cleaning process is to select all of the PMTs with signal while rejecting all PMTs with noise alone. We have simulated 500 images (incident energy 143 GeV) and determined the number of signal PMTs correctly selected and the number of noise PMTs incorrectly selected. These results are shown in Figure 3.

High energy gamma-ray showers produce large, bright images which result in a greater number of PMTs being selected. This is adequate for the characterization of the image shape and orientation used for discriminating gamma-rays

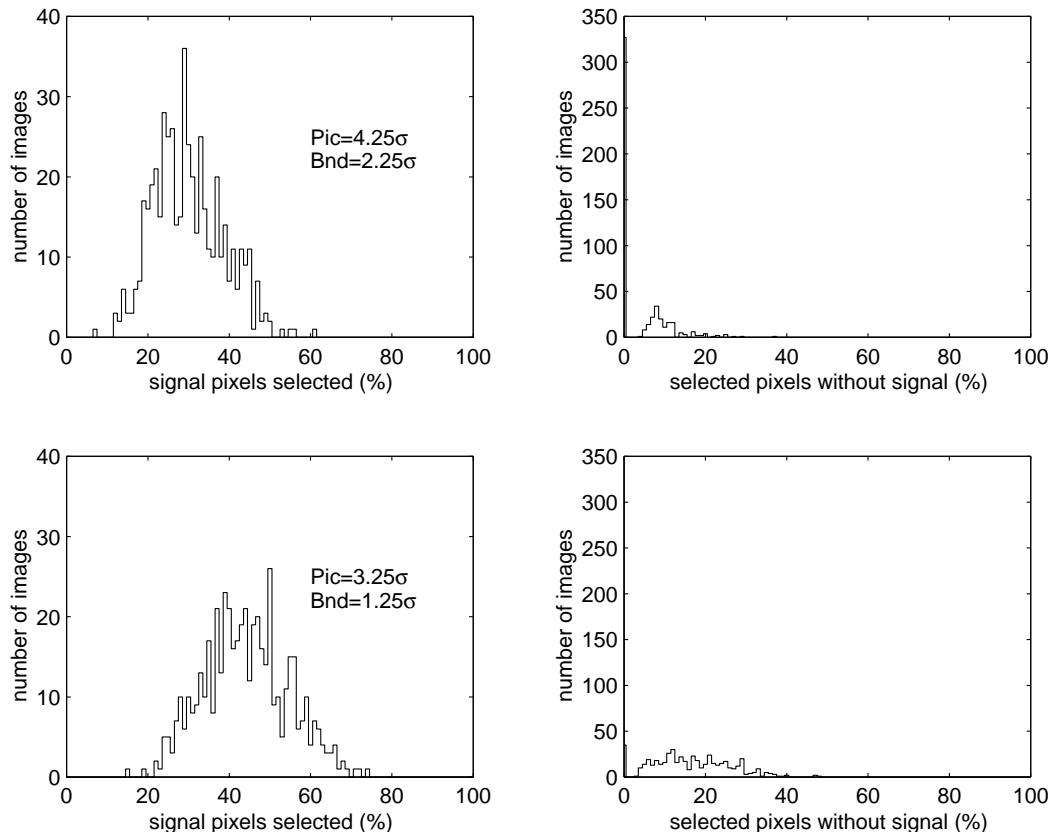


Fig. 3. (Top) Distribution of the number of (Left) signal pixels selected which have at least one Cherenkov photon, relative to the total number selected. The right panel shows the number of pixels selected without signal, i.e. noise (zero Cherenkov photons), relative to the total number selected. In both panels, the traditional method of picture boundary thresholds given in the text was used. (Bottom) The same distributions but utilizing lower picture boundary thresholds.

from the more numerous hadrons. However, for low energy showers, only a few PMTs are selected by the traditional method resulting in a poor reconstruction of the image. Relaxing the thresholds includes too many noise PMTs, as shown in Figure 3, resulting in increased error in the reconstruction which affects the sensitivity, energy and angular resolution of ACT telescopes operating at low energies.

3 Wavelet Method

Wavelet techniques are developing rapidly and are proving to be very efficient as signal and image processing methods. These techniques have been applied in different fields and in particular in astrophysics and cosmology. Among the myriad of papers, examples of the detection of structure in astrophysical and cosmological images using wavelets can be found in (11; 12; 13; 14). De-

noising and compression of astrophysical and cosmological images have also been performed using wavelet techniques (15; 16; 17). Wavelets are also a useful tool for performing statistical analysis, for example see (18; 19). As previously described, the cleaning and characterization of Cherenkov images are not easy tasks and have to be performed by applying well adapted methods. Wavelets are just now being utilized to analyse these images. Wavelet moments were introduced as a complementary method to characterize Cherenkov images in (20). Wavelets could as well be used to clean and characterise Cherenkov images at the same time. In this work, we will use wavelets, in a novel way, only to select pixels containing Cherenkov photons. That is, wavelets will be used for the cleaning process. A Hillas parametrisation will afterwards provide the characterisation of the images.

3.1 Image Processing Using Wavelets

We have developed a wavelet based method to select signal pixels in atmospheric Cherenkov images. Wavelet decomposition of an image provides information about the contribution of different scales to each pixel. The combined information at several scales at each location in the image makes wavelet methods a very powerful technique. Wavelet coefficients $wv(R, \vec{b})$ are calculated for a fixed scale R at each pixel \vec{b} , by convolving the image under analysis $f(\vec{x})$ with a wavelet $\Phi = \Phi(\vec{x}, R)$:

$$wv(R, \vec{b}) = \int d\vec{x} f(\vec{x}) \Phi\left(\frac{|\vec{x} - \vec{b}|}{R}\right). \quad (1)$$

The method we use to separate the noise from the signal relies on the characteristics of the noise rather than on the characteristics of the signal. These characteristics will be determined by the distributions of wavelet coefficients corresponding to noise, at several scales. As one of the possible analyzing wavelets, we have chosen the so called Mexican Hat wavelet given by

$$\Phi\left(\frac{|\vec{x} - \vec{b}|}{R}\right) = \left(2 - \frac{|\vec{x} - \vec{b}|^2}{R^2}\right) e^{-\frac{|\vec{x} - \vec{b}|^2}{2R^2}} \frac{1}{(2\pi)^{0.5} R}. \quad (2)$$

An isotropic wavelet such as the Mexican Hat seems more appropriate for this analysis than an anisotropic one, since we do not want any direction to be preferred by the wavelet coefficients.

As previously mentioned, the method designed to select signal pixels in our images takes into account the *a priori* information about the characteristics of the noise. The pedestal and pedestal variance for each pixel are deter-

mined as described in §2.1. The noise at each location is approximately described by a Gaussian distribution with pedestal mean, and variance equal to the pedestal variance. A characterisation of the noise distribution affecting Cherenkov images was presented in figure 3 in (8). As one can see the fit to a Gaussian distribution is very good. We generate 300 noise simulations (determined to be a sufficient number of simulations to reproduce the distributions; this number is a good compromise between accuracy and computational speed) and for each simulation we calculate the wavelet coefficients corresponding to four different scales, multiples of the characteristic pixel scale $R = 2 \times pix_size, 3 \times pix_size, 4 \times pix_size, 5 \times pix_size$. At each pixel and each scale we generate the wavelet coefficient probability distributions corresponding to noise.

Once the noise wavelet coefficient distributions are known at each location of the image for the four scales the wavelet coefficients corresponding to the image under analysis are calculated for the same four scales. In the second step a probability is assigned to each of these wavelet coefficients by comparing their values with the corresponding noise wavelet coefficient distribution. Finally only those pixels with wavelet coefficients outside the noise wavelet coefficient distributions at all scales are selected. The use of several scales in the wavelet method has the advantage of using information about the noise not only in the pixel under analysis (as the traditional picture-boundary selection method) but in the neighbouring pixels. Note, that this is not the way in which wavelets are normally used to separate signal from noise. In a “classical” approach wavelet coefficients at scales dominated by noise (the smaller ones) are thresholded (hard or soft thresholding). The image is afterwards reconstructed based on these “modified” wavelet coefficients. This is in brief, the “classical” denoising procedure using wavelets. We would like to remark that we are not denoising the images. Wavelets are here used to select pixels containing Cherenkov photons. Noise will still be present in the image afterwards characterised with Hillas parameters.

3.2 Results

The same Monte Carlo simulations used to test the performance of the traditional cleaning procedure are now utilized to determine the characteristics of the wavelet method. Figure 4 shows the same images depicted in Figure 2, but cleaned with the wavelet method. This procedure selected significantly more signal pixels than the picture boundary method, while at the same time, selecting only a few pixels which do not contain signal due to Cherenkov light from the air shower. For the image on the left, 57% of the signal pixels are selected, compared to the 25% selected by the traditional method, as shown in Figure 2. For the image on the right 65% of the signal pixels are selected com-

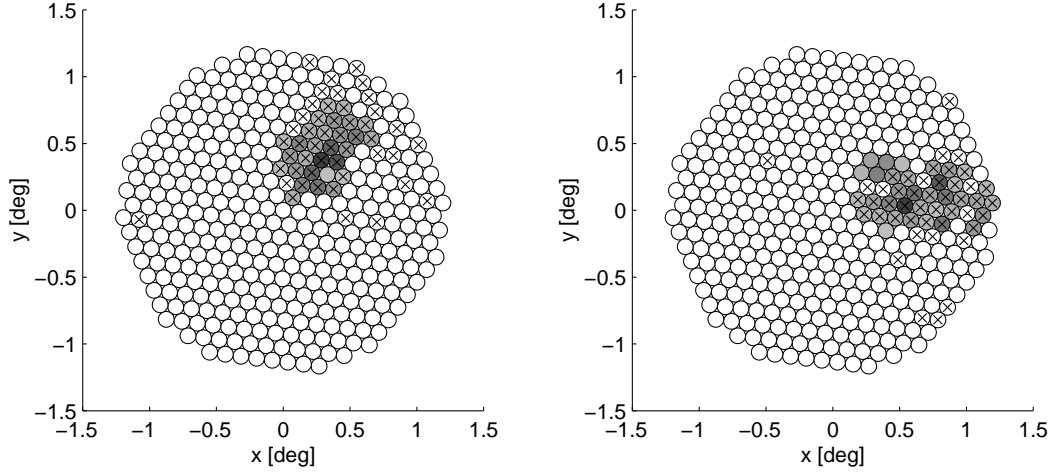


Fig. 4. The same sample images shown in Figure 2 but cleaned using the wavelet method given in the text. Pixels selected by this technique are shaded in gray scale with darker shades corresponding to greater ADC signal for that PMT. The cross symbols denote pixels with at least one photoelectron due to Cherenkov light.

pared to the 7% selected by the traditional method, as shown in Figure 2. The distribution of the number of signal pixels selected and the number of noise pixels erroneously chosen for 500 simulated gamma-ray images are depicted in Figure 5. Clearly, the wavelet method includes more of the Cherenkov light signal than the traditional method of picture boundary thresholds. This results in a greater number of available pixels to reconstruct the characteristics of the Cherenkov light image. The pixels selected by this method and not by the traditional method must have small signal and thus greater noise contribution. The pulse height distribution for a single pixel is represented in Figure 6. The pulse height is the sum of signal and noise contributing to a pixel. The noise is approximately Gaussian in shape. The signal lies under the noise distribution and is responsible for the tail at larger pulse heights. As one can see in the top panel, the picture boundary thresholds indiscriminately discard pulses below the fixed threshold, some with genuine signal, albeit small. On the other hand, the wavelet cleaning method selects more pulses with a few well inside the noise distribution. This is a result of the wavelet method including more information about the spatial distribution of the noise, and not just the noise itself, thereby allowing the inclusion of pixels with low signal to noise contributions. It is this property that makes the wavelet method optimal for subsequent image reconstruction and characterization based on Hillas parameters.

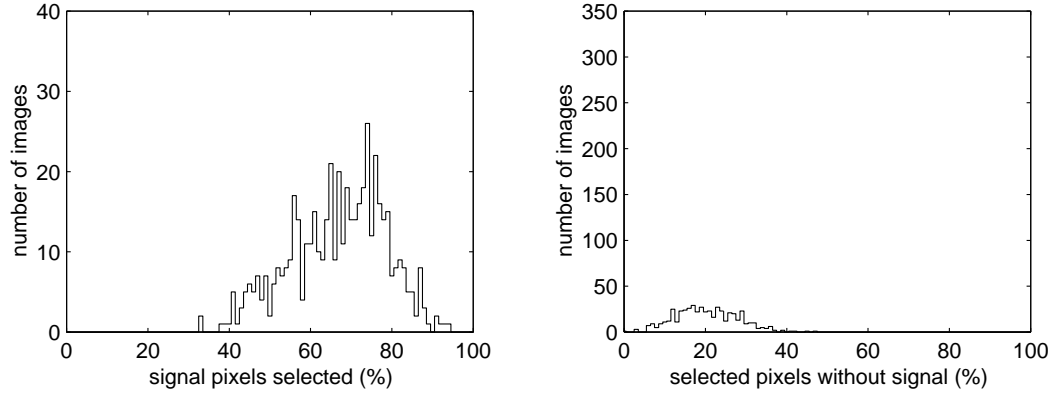


Fig. 5. Distribution of (Left) the number of selected signal pixels relative to the total number of selected pixels and (Right) the number of selected pixels without signal, i.e. noise, relative to the total number of pixels selected, using the wavelet method given in the text.

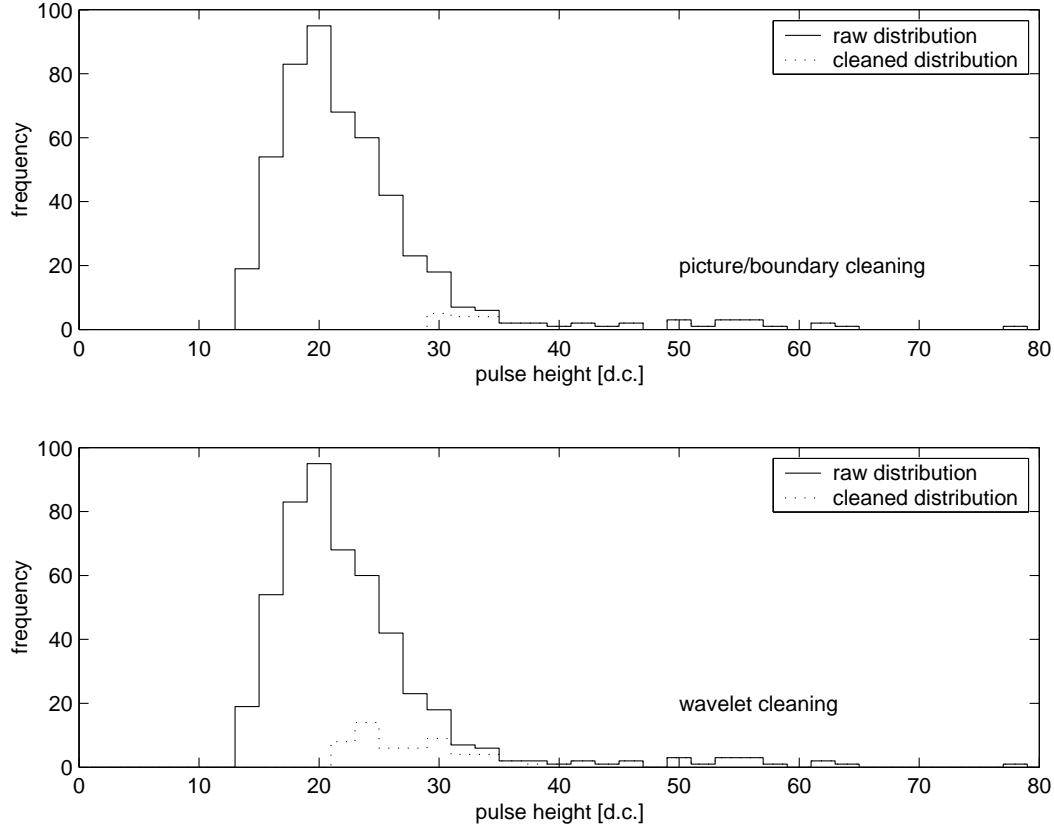


Fig. 6. Distribution of pulse height of a pixel before (solid line) and after (dotted line) applying a cleaning method. The result of applying the picture/boundary method is presented in the top panel. Wavelet cleaning results in the pulse height distribution shown in the bottom panel.

Table 1

Definition of image parameters, used to characterize the image shape and orientation in the FOV (see Figure 7).

| Parameter | Definition |
|------------|--|
| max1: | largest signal recorded by the PMTs. |
| max2: | second largest signal recorded by the PMTs. |
| size: | sum of all signals recorded. |
| centroid: | weighted center of the light distribution (x_c, y_c) . |
| width: | the RMS spread of light along the minor axis of the image; a measure of the lateral development of the shower. |
| length: | the RMS spread of light along the major axis of the image; a measure of the vertical development of the shower. |
| distance: | the distance from the centroid of the image to the center of the FOV. |
| α : | the angle between the major axis of the image and a line joining the centroid of the image to the center of the FOV. |
| asymmetry: | the skewness of the light distribution relative to the image centroid. |

4 Image Reconstruction and Characterization

Each Cherenkov image is characterized using a moment analysis (22). The roughly elliptical shape of the image is described by the length and width parameters. Its location and orientation within the FOV are given by the distance and α parameters, respectively. The asymmetry parameter, defined as the third moment of the light distribution, describes the skew of the image along its major axis. Also determined are the two highest signals recorded by the PMTs (max1, max2) and the amount of light in the image (size). These parameters are defined in Table 1 and are shown in Figure 7. These are called Hillas parameters (7).

Gamma-ray events give rise to shower images which are preferentially oriented towards the source position in the image plane. These images are narrow and compact in shape, elongating as the impact parameter increases. They generally have a cometary shape with their light distribution skewed towards their source location in the image plane. Hadronic events give rise to images that are,

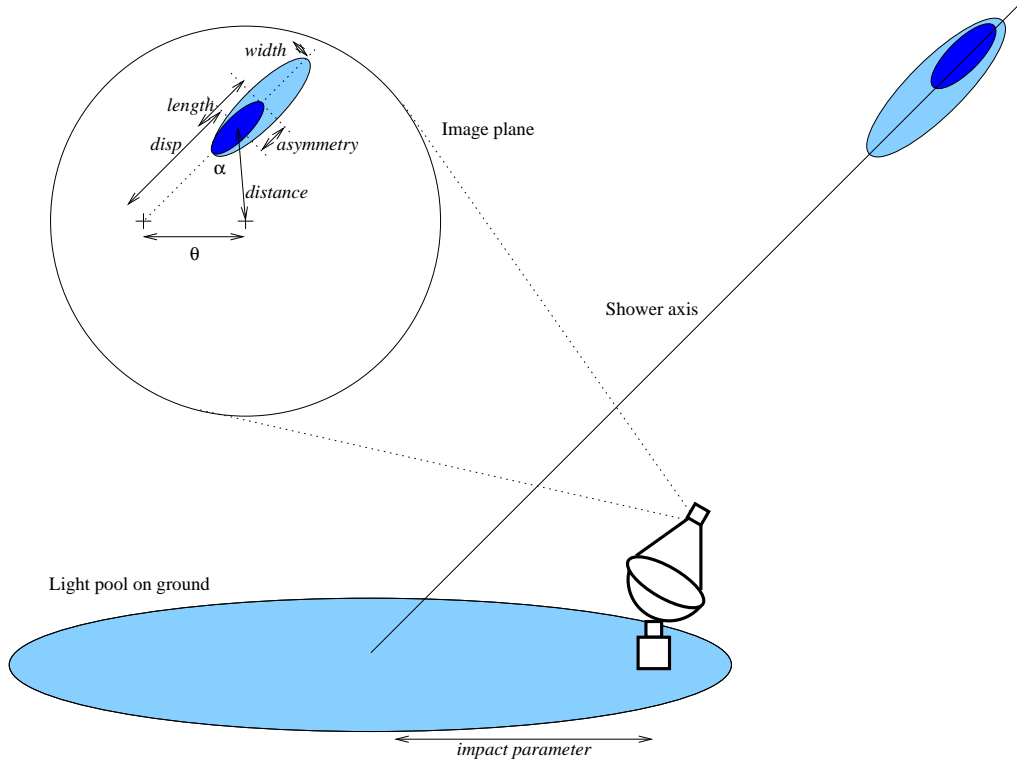


Fig. 7. Depiction of the light produced by air showers. The image plane shows the definition of the Hillas parameters used to characterize each image.

on average, broader (due to the emission angles of pions in nucleon collisions spreading the shower), and longer (since the nucleon component of the shower penetrates deeper into the atmosphere) and are randomly oriented within the FOV. Utilizing these differences, a gamma-ray signal can be extracted from the large background of hadronic showers.

Monte Carlo simulations of gamma-ray induced air showers are used to visualize the effect of wavelet cleaning on the moments of the light distribution. Firstly, as depicted in Figure 8, the wavelet cleaned images tend to have greater size and a lower concentration of light in the brightest three pixels (called frac3). These are simply due to the inclusion of a greater number of signal pixels in the image. Secondly, for the same reason, the images tend to be wider and longer as shown in Figure 8. Also noted in this figure is that the width and length distributions for the wavelet cleaned images are more symmetric and lack the long tails at large values of width and length as found with the picture-boundary cleaned images. These tails are likely the result of “hot” single pixels which grossly distort the image. Lastly, images are selected as gamma-ray candidates if they have small α values and positive asymmetry. The greater number of pixels selected by the wavelet cleaning method enables a more accurate determination of both of these quantities as shown in Figure 8. When extracting a gamma-ray signal from a background of hadronic

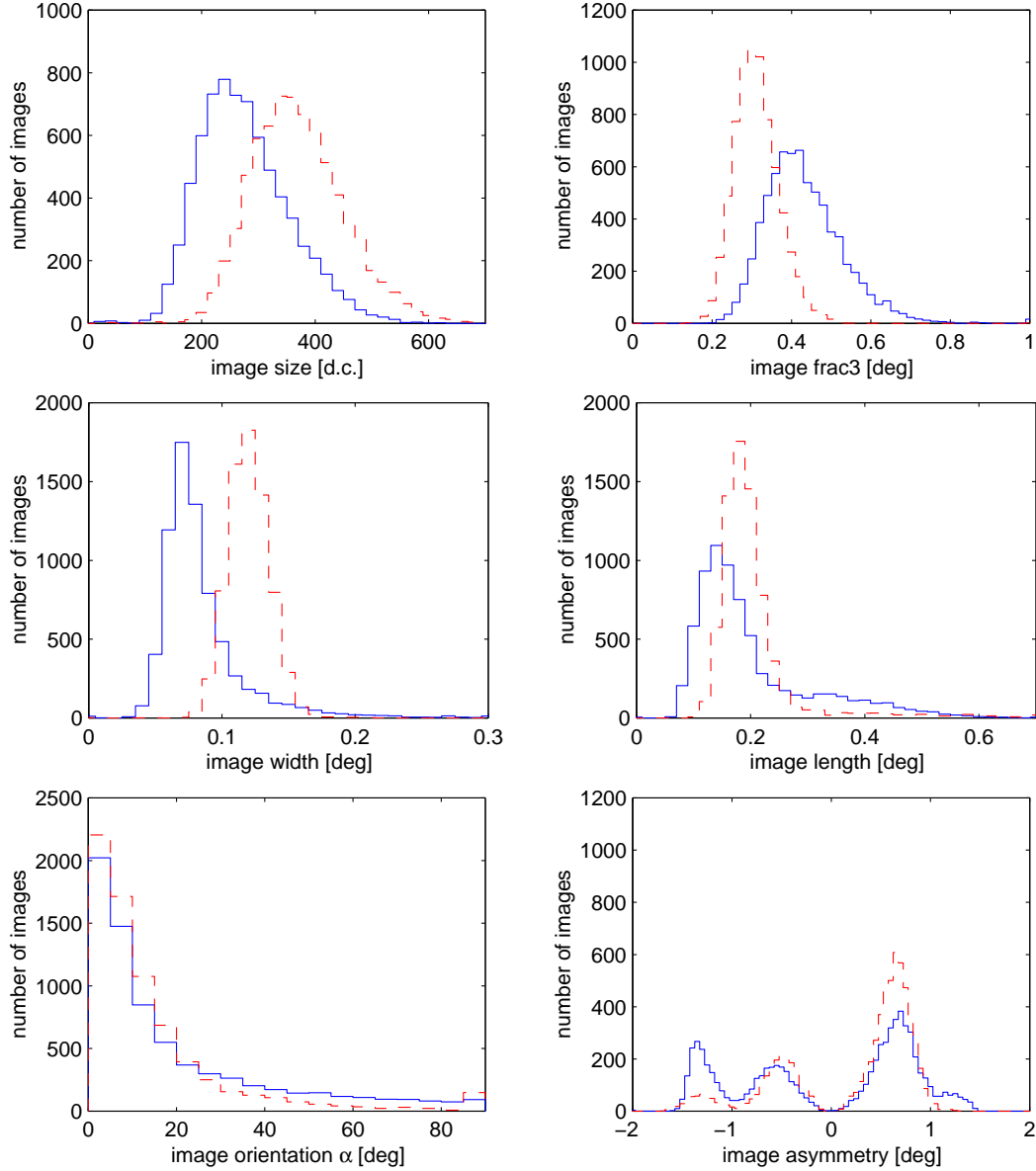


Fig. 8. Distribution of the Hillas parameters for 7156 Monte Carlo simulations of 150 GeV gamma-ray induced air showers. Results from the traditional picture-boundary cleaning method are shown as solid lines. Results from the wavelet cleaning method are shown as dashed lines.

images, a selection of $\alpha < 15^\circ$ and asymmetry > 0 is made. In the case of the α selection, the wavelet method collects 15% more images. When combined with the asymmetry selection 33% more images are collected due to the improved reconstruction.

4.1 *Application to observations taken on established sources*

The efficacy of utilizing wavelets as a method for image processing for imaging Atmospheric Cherenkov telescopes can be verified by applying the technique to observations of established sources such as the Crab Nebula, the standard candle for ground-based gamma-ray astronomy. We compare our results to traditional analysis methods used by the Whipple Collaboration and outlined in (8). The traditional analysis technique consists of the image processing methods described in this paper, including the application of picture and boundary thresholds for image cleaning, followed by characterization and image selection criteria known as Supercuts (22). These selection criteria, preferentially select gamma-ray induced images from the much more numerous hadronic images. Our comparison follows the same techniques however, the images will be cleaned with the wavelet method described herein.

As previously described, wavelet cleaning is expected to provide improved performance for low energy events, where the number of signal pixels selected by traditional methods is small and thus prone to greater errors in the reconstruction. In fact, Supercuts are optimized for peak sensitivity discarding many low energy images, as they cannot be distinguished from single muon images and noise. As shown in Figure 9., the peak in the distribution of image size selected by Supercuts is 550 d.c., accordingly for comparison, we choose to focus on images below this size.

Our comparison requires two distinct procedures. Firstly, image selection cuts must be optimized for both the picture boundary and wavelet cleaning methods. Note that cuts for the picture boundary cleaning method are re-optimized from traditional values due to the introduction of a size limitation which alters the optimum cuts, see (6) for an in depth discussion. Secondly, these new criteria must be tested on an independent data set to alleviate any bias due to optimization. In addition, for this analysis, we determine image size using a common definition to ensure that the same events are included in both cases; for these results image size was calculated from the picture boundary cleaned image.

The optimization procedure involves bounding all but one selection criterion whilst searching for optimum signal to noise performance via standard grid search methods. We define signal to noise performance as the number of standard deviations the signal appears above background. We have chosen a set of observations on the Crab Nebula, taken under good sky conditions and instrument operations. A total of 12 hours of data, taken over the period December 1999 to January 2000, are included. The results are shown in Figure 10 and given in Table 2. The order that each parameter is optimized is as shown in Figure 10, starting from the top and working left to right. Before each pa-

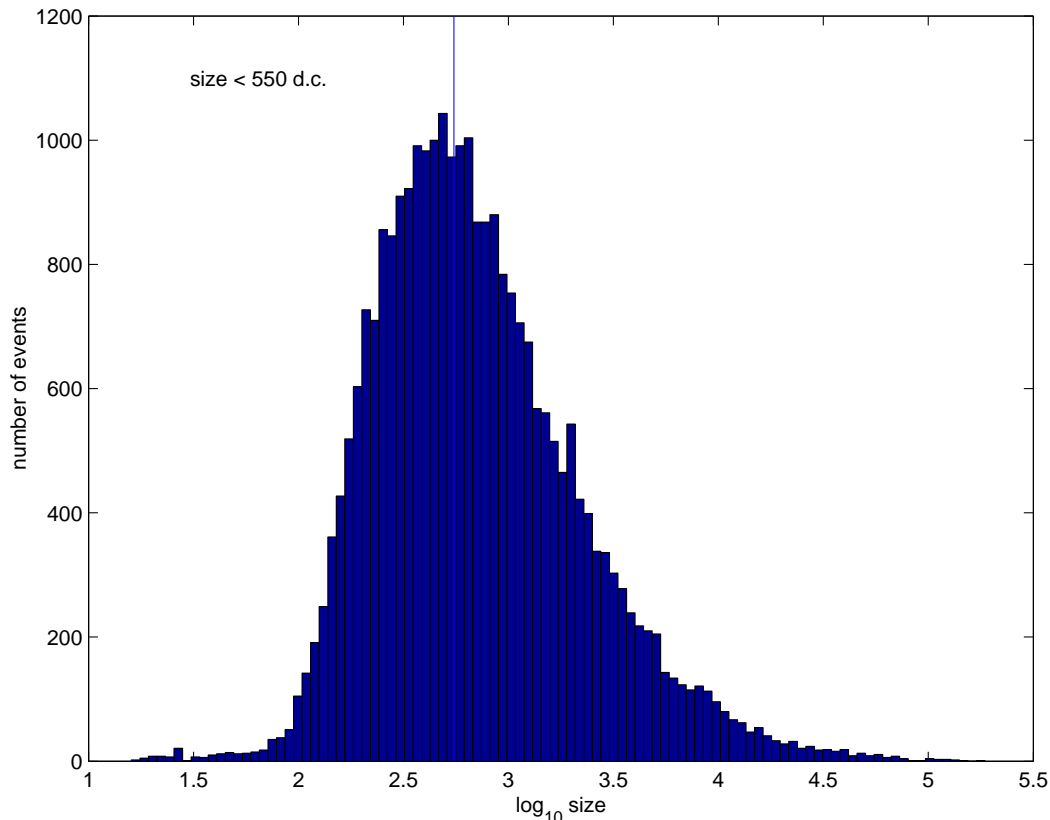


Fig. 9. The distribution of image size as derived from images cleaned with the traditional method of picture boundary thresholds. The vertical line indicates the upper bound in size chosen for the analysis.

parameter is optimized the traditional cut parameters were chosen, as given in Table 2. Upon the determination of an optimum cut, this new value is used for the remaining procedure. This method has been the standard practice of optimization by the Whipple Collaboration over the past decade and has been found to be more effective than other optimization methods such as the Simplex algorithm.

The results of the optimization indicate enhanced reconstruction capabilities as shown by the inclusion of events at all lower distances and a lower cut of the image pointing angle α . Supercuts typically discard images at lower distance due to the potential for greater error in the calculation of the image pointing angle α .

These results cannot be used to compare performance due to the optimization bias. As a result we have analyzed a set of observations taken on the Active Galactic Nuclei Markarian 421 and 501, long established as gamma-ray sources (23; 24). A total of 5 hours of data, taken between January 2000 and May 2000, under good sky and instrument operation, are included (data from Markarian 421 and 501 are gathered together to provide a good unbiased source of VHE

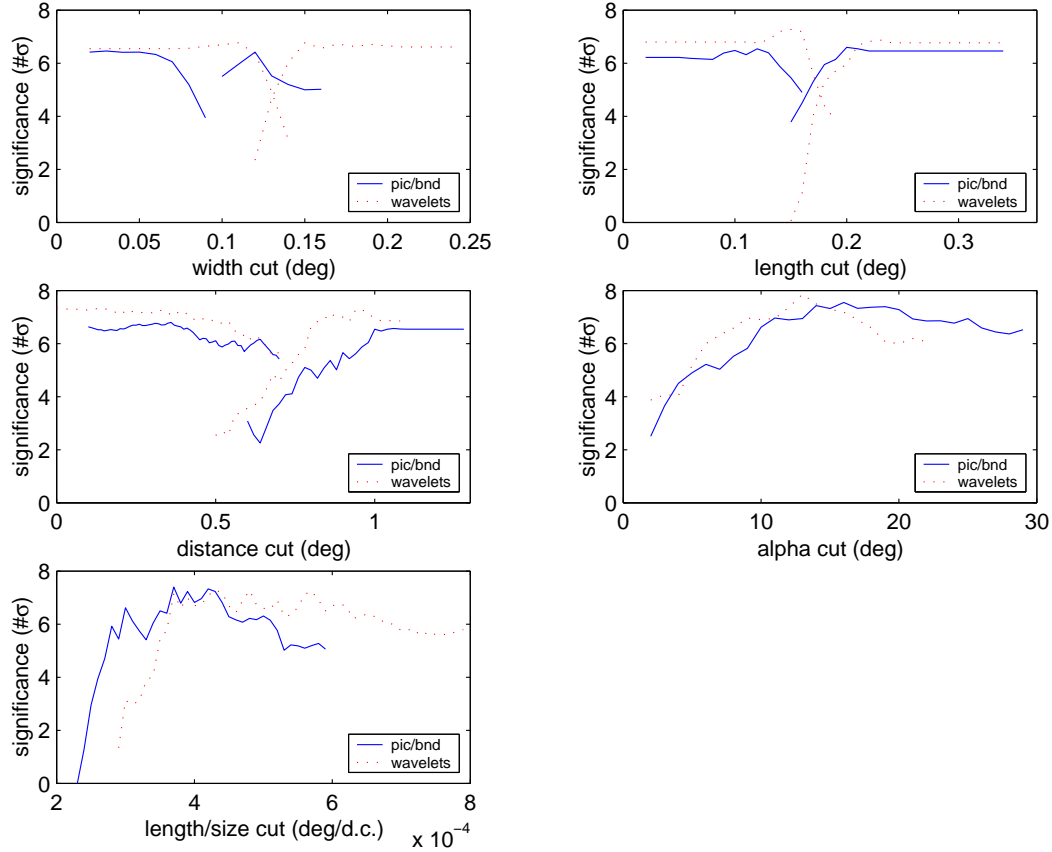


Fig. 10. Optimization of image selection cuts. The results for the data cleaned with the traditional picture boundary thresholds are shown as solid curves. The results for the data cleaned with wavelets are shown as dashed curves. The two independent branches appearing in the width, length and distance plots correspond to the optimization of the lower and upper limits.

Table 2

Supercuts selection criteria, which were optimized on contemporaneous Crab Nebula data.

| Traditional supercuts 2000 | Low Energy Images Pict/Bound Cleaned | Wavelet Cleaned |
|-------------------------------|---|------------------------|
| size > 0 | 0 < size < 550 | 0 < size < 550 |
| max2 > 30 | max2 > 30 | max2 > 30 |
| 0.05 < width < 0.12 | 0.03 < width < 0.12 | 0.11 < width < 0.15 |
| 0.12 < length < 0.25 | 0.12 < length < 0.21 | 0.15 < length < 0.23 |
| 0.40 < distance < 1.00 | 0.36 < distance < 1.00 | 0.00 < distance < 0.94 |
| $\alpha < 15$ | $\alpha < 16$ | $\alpha < 13$ |
| length/size < 0.00040 | length/size < 0.00042 | length/size < 0.00057 |

Table 3

Results of the analysis of data taken on the Active Galactic Nuclei, Markarian 421 and 501. The increase in gamma-ray rate is the result of larger collection area at low energies afforded by the wavelet technique. In the traditional method these photons would have been discarded due to lack of signal after cleaning thus lowering collection area / efficiency.

| Image Cleaning Method | ON source counts | OFF s.c. | Excess (# of σ) | Rate (/min) |
|--------------------------|---------------------|----------|-------------------------|---------------|
| Picture/Boundary | 1446 | 1219 | 4.39 | 0.74 +/-0.17 |
| Wavelets | 2254 | 1902 | 5.46 | 1.02 +/- 0.21 |

photons). The data used spanned the same range of elevation as the Crab data. All sets of data were taken at small zenith angles (zenith angle dependence is too small to measure). The results, given in Table 3, show the expected increase in collection area for low energy events, afforded by the wavelet method.

5 Conclusions

The imaging atmospheric Cherenkov technique has pioneered the detection of VHE gamma-rays from ground-based observatories. The main difference remaining between space-based and ground-based gamma-ray observatories is the detection of gamma rays in the 10 to 200 GeV energy band. Photons in this energy range are too few for the limited collection areas of space-based instruments and typically produce low levels of Cherenkov light for a single reflector at ground level. The aim of this paper was to present a novel cleaning method based on wavelets that increases the number of signal pixels selected while rejecting the maximum number of noise pixels.

The traditional cleaning method used to analyse images provided by Cherenkov telescopes selects those pixels which are above the picture threshold ($4.25 \times \text{RMS}$) or are beside such pixels and have signal above the lower neighbour threshold ($2.25 \times \text{RMS}$). The performance of a cleaning method can be viewed using Monte Carlo simulations. Figures 2 and 3 show these results in the case of the traditional image cleaning method. Only a small percentage (average of $\sim 30\%$) of the total number of PMTs that have real signal are selected by this method. The percentage can be increased by lowering the picture and boundary thresholds. However, this also increases the number of noise pixels incorrectly selected as signal pixels (see bottom panels in Figures 2 and 3).

A method to select a greater number of real signal pixels, while excluding pixels with noise alone has been presented in this work. The method is based

on the significant property of wavelets of providing information about the contribution of different scales to each location of an image. This is a novel method and it is important to notice that denoising is not carried out. Convolution of an image with a wavelet of certain size will provide a new image (in wavelet space) with information at each pixel of the contribution of the scale given by the wavelet size. The Mexican Hat wavelet was chosen for this work based on its isotropy. Assuming the noise in each pixel comes from a Gaussian distribution of well characterized mean and variance, we build the probability distribution of noise wavelet coefficients at four scales. Comparison of the wavelet coefficients obtained for the image at the four analysed scales with the noise wavelet coefficient distributions allows us to discriminate between signal and noise dominated pixels. As shown in Figures 4 and 5 the percentage of signal selected pixels (average of $\sim 70\%$) has increased compared to the traditional cleaning method. At the same time the number of erroneously selected pixels has only slightly increased.

The fact that the wavelet method selects a larger number of pixels improves the image reconstruction and characterization. The wavelet method provides a better determination of α and asymmetry as shown in Figure 8. Moreover, this method proves to be very promising in extracting the signal of low-energy events. A noticeable difference between the wavelet and the traditional methods can be observed in the results obtained from Markarian 421 and 501 data as presented in Table 3. Moreover, the increased number of pixels selected by the wavelet cleaning method may prove to be of advantage for selection methods not based on simple moments of the light distribution, for example the method developed for the fine pixel camera utilized by the CAT experiment (25). Such methods do not assume simply ellipsoidal image structure and thus can take better advantage of finer details, at several scales, of the wavelet cleaned images.

We would like to stress the fact that for a single telescope the limiting factor for discriminating low energy events is still muons, with or without wavelet cleaning. This problem will only be solved by the construction of arrays of Cherenkov imaging telescopes as HEGRA (26) and the one proposed by the VERITAS project (27). For an array of telescopes muons will not trigger the instrument. Therefore in this case, the limiting factor will be the number of pixels passing the clean-up routine and hence a wavelet image cleaning method as the one presented in this paper will be of great advantage.

Acknowledgements

The authors thank A. Haungs, S. LeBohec and T. Palfrey for useful comments. This research is supported by grants from the U.S. Department of Energy. We

thank the Whipple Gamma-ray Collaboration for the use of the data presented in this paper. L.C. thanks the Department of Physics at Purdue University for its hospitality during her visits.

References

- [1] T.C. Weekes, et al., *ApJ* 342 (1989) 379.
- [2] S.M. Bradbury, et al., *Proceedings of the 2xth International Cosmic Ray Conference*, vol 5, Salt Lake City, USA, 1999, p. 263.
- [3] R.W. Lessard, et al., *Astropart Phys* 15 (2001) 1.
- [4] A. Barrau et al., *Nucl. Instr. and Meth. A* 416 (1998) 278-292.
- [5] M. Catanese, et al., *Proceedings Towards a Major Atmospheric Cherenkov Detector IV*, Padova, Italy, 1995, p. 335.
- [6] P. Moriarty et al., *Astropart Phys* 7 (1997) 315-327.
- [7] A.M. Hillas, *Proceedings of 19th International Cosmic Ray Conference*, vol. 3, La Jolla, USA, 1985, p. 445.
- [8] D.J. Fegan, et al., *Proceedings Towards a Major Atmospheric Cherenkov Detector III*, Tokyo, Japan, 1994, p. 149.
- [9] M. Kertzman, G.H. Sembroski, *Nucl. Instr. and Meth. A* 343 (1994) 629-643.
- [10] G. Mohanty, et al., *Astropart Phys* 9 (1998) 15.
- [11] F. Damiani, A. Maggio, G. Micela and S. Sciortino, *ApJ* 483 (1997) 350-369.
- [12] J. Krywult, H.T. MacGillivray, and P. Flin, *A&A* 351 (1999) 883-892.
- [13] D. Lazzati, S. Campana, P. Rosati, M.R. Panzera and G. Tagliaferri, *ApJ* 524 (1999) 414-422.
- [14] L. Cayón, J.L. Sanz, R.B. Barreiro, E. Martínez-González, P. Vielva, L. Toffolatti, J. Silk, J.M. Diego and F. Argüeso, *MNRAS* 315 (2000) 757-761.
- [15] J.L. Sanz, F. Argüeso, L. Cayón, E. Martínez-González, R.B. Barreiro and L. Toffolatti, *MNRAS* 309 (1999a) 672-680.
- [16] J.L. Sanz, R.B. Barreiro, L. Cayón, E. Martínez-González, G.A. Ruiz, F.J. Díaz, F. Argüeso, J. Silk and L. Toffolatti, *A&AS* 140 (1999b) 99-105.
- [17] L. Tenorio, A.H. Jaffe, S. Hanany, and C.H. Lineweaver, *MNRAS* 310 (1999) 823-834.
- [18] M.P. Hobson, A.W. Jones, and A.N. Lasenby, *MNRAS* 309 (1999) 125-140.
- [19] R.B. Barreiro, M.P. Hobson, A.N. Lasenby, A.J. Banday, K.M. Gorski and G. Hinshaw, *MNRAS* 318 (2000) 475-481.
- [20] A. Haungs, et al., *Astropart Phys* 12 (1999) 145-156.
- [21] M.F. Cawley, et al., *Exper. Astr.* 1 (1990) 173.
- [22] P.T. Reynolds, et al., *ApJ* 404 (1993) 206.

- [23] M. Punch et al., Nature 358 (1992) 477.
- [24] J. Quinn, et al., ApJ 456 (1996) L83.
- [25] S. LeBohec, et al., NIM A416 (1998) 425.
- [26] HEGRA Collaboration; A. Konopelko et al., Astropart Phys 10 (1999) 275.
- [27] R. Lessard, Astropart Phys 11 (1999) 243.